Modelling Dynamic Fracture and Flow in Jointed Rock by Blasting

H Sakaguchi[1], H-B Mühlhaus[1] and Y Wei[1]

ABSTRACT

Particles are by far the easiest objects to simulate, because their dynamics is simple. Determining the motion of particles and their interaction, a wide variety of deformable structures can be constructed by connecting particles that have mass, position, and velocity, and that respond to forces. Starting from this simple idea we have derived what we call the particle-lattice method for the solutions of boundary value problems of deformation and fracture of solid mass. The problem of rock breaking by blasting operations as well as fracture and flow of rocks fragments involve momentum transfer between solid and fluid; gas flow and reactive mass transfer. In this paper we outline the method and describe briefly the salient features of the algorithm. We derive relationships between the contact properties for the discrete model and the properties of the underlying continuum and fluid flow coupling procedure. Finally we illustrate the potential of the method by means of example solutions related to the dynamic fracture and flow in jointed rock by blasting.

INTRODUCTION

The safe execution of many mining processes including blasting, caving and minerals processing requires the availability of predictive simulation tools for dynamic fracture and flow of brittle materials. Such simulations can in principle predict accurately the workings of complex processes and allow variation in many parameters to be evaluated before expensive technology is employed in constructing or designing the optimal choice.

The main obstruction to modelling geomechanics and solving mining problems has been the lack of appropriate numerical tools to handle the difficulties arising from material inhomogeneity, brittle fracture and the associated complex damage patterns. The application of grid based discretisation procedures, such as the finite element method, can be problematic even if the material is macroscopically homogeneous, if for instance large deformations are involved. In this case purely Lagrangian methods can become tangled or require unreasonably small time steps to be successful. Remeshing (eg Carter *et al*, 1995) is problematic if fracturing occurs on more than one scale or where history dependency is involved. For these reasons, particle based methods for solid mechanics seem to be increasing in popularity (Libersky *et al*, 1993; Belytschko *et al*, 1994; Sulsky *et al*, 1995).

In related developments, Jirásek and Bazant (1993), Song and Kim (1995), and van Mier *et al* (1995) model static and dynamic fracture of brittle materials by a combination of discrete element and lattice network methods. From a mathematical view point discrete element based particle methods may be interpreted in the spirit of Smooth Particle Hydrodynamics (SPH, eg Libersky *et al*, 1993) with discontinuous Kernel functions.

In the following section we give a brief outline of the salient physical and computational features of the particle-lattice method. The basic idea is simple enough: The infinite number of material points of the continuum is replaced by a finite number of 'pseudo particles', each of which occupies a spherical volume. The mechanical properties of the solid (yield criteria, elasticities, etc) are applied at the surfaces of the pseudo particles. In addition, we present a hybrid formulation for coupled fluid-solid deformation scheme to deal with pore fluid and gas flow in the rock matrix and in the fractured rock. In the last section, the potential of the method is illustrated by means of example solutions related to granular flow, and blasting in jointed rock as a part of gas flow coupling.

1. CSIRO Division of Exploration and Mining, Rock Mechanics Research Centre, CSIRO Division of Exploration and Mining, 39 Fairway (PO BOX 437), Nedlands WA 6009.

FORMULATION

In this study, rocks are basically described as assemblies of bonded particles. The procedure for the establishment of the domain of each boundary value problem, and the solutions of the equations of motion are similar to the ones employed in the discrete element method (Cundall and Strack, 1979). However in the contact search algorithm, advantage is taken of the fact that in solid mechanics problems, most of the contacts are permanent (see, eg Sakaguchi, 1995 for details). In the following we first give a brief description of the assumed interaction relationships between particles and then turn to an outline of the fluid flow coupling scheme which is essential to blasting simulation.

Contact mechanics and yield criterion

We consider two granules i and j having translational velocities $\mathbf{v}^i$ and $\mathbf{v}^j$ and angular velocities $\mathbf{s}^i$ and $\mathbf{s}^j$. Continuum versions of the following formulations have been derived by Mühlhaus and Oka (1996) and Mühlhaus and Hornby (1997). The relative velocity (Figure 1) at the contact is:

$$\mathbf{g}^{ji} = \mathbf{v}^{ji} + d^{ji}\mathbf{n}^{ji} \times \mathbf{s}^{ji}, \tag{1}$$

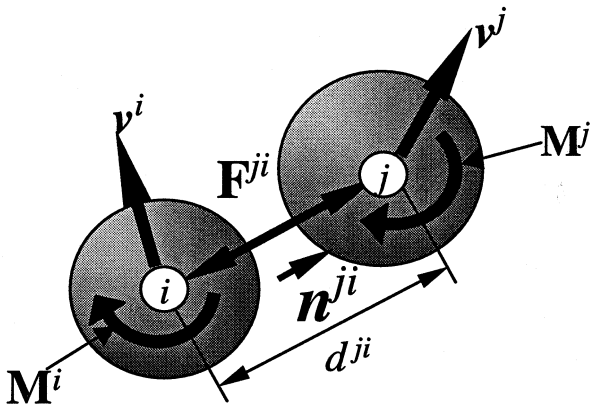

FIG 1 - Contact geometry for spherical particles.

where $\mathbf{v}^{ji} = \mathbf{v}^j - \mathbf{v}^i$, $\mathbf{s}^{ji} = \mathbf{s}^j + \mathbf{s}^i$, $\mathbf{n}^{ji}$ is the unit vector along the connecting line between the mass centres of the granules and d^{ji} is the distance between the mass centres. To facilitate the treatment of non-linear particle interactions we formulate the

constitutive relationships of the contacts in rate from. The relevant co-rotational rates of the contact force ($\overset{\nabla}{\mathbf{F}}^{ji}$) and moment ($\overset{\nabla}{\mathbf{M}}^{ji}$) vectors read:

$$\overset{\nabla}{\mathbf{F}}^{ji} = \dot{\mathbf{F}}^{ji} - \mathbf{W}^{i}\mathbf{F}^{ji} \tag{2}$$

$$\overset{\nabla}{\mathbf{M}}^{ji} = \dot{\mathbf{M}}^{ji} - \mathbf{W}^{i}\mathbf{M}, \tag{3}$$

where

$$\mathbf{W}^{ji}_{\alpha\beta} = \frac{1}{2}\varepsilon_{\alpha\beta\gamma}\left(s^{i}_{\gamma} + s^{j}_{\gamma}\right)$$

and $\varepsilon_{\alpha\beta\gamma}$ denotes permutation symbol. It should be noted that there are other acceptable definitions of $\mathbf{W}^{ji}$ in Equations 2 and 3. One could for instance define $\mathbf{W}^{ji}$ as the spin of the connecting line between the mass centres of the particles *i* and *j*. However, such a definition is effective only for the contact forces and the bending moments. The increments of the torsional moments $\mathbf{M}^{ji}{}_{\alpha\beta}\mathbf{n}^{ji}{}_{\alpha}\mathbf{n}^{ji}{}_{\beta}$ would have to be treated separately. The present definition applies for torsinal moments as well. The overdot on **F** and **M** denotes time derivatives of the contact force and moment respectively. Elastic contacts are described in the simplest possible way as:

$$\overset{\nabla}{\mathbf{F}}^{ji}_{el} = K_{s}(\mathbf{g}^{ji} - (\mathbf{g}^{ji}\cdot\mathbf{n}^{ji})\mathbf{n}^{ji}) + K_{n}(\mathbf{g}^{ji}\cdot\mathbf{n}^{ji})\mathbf{n}, \tag{4}$$

$$\overset{\nabla}{\mathbf{M}}^{ji}_{el} = d^{ji\,2}K_{r}(s^{j} - s^{i}) \tag{5}$$

where K_s, K_n and K_r are constant tangent, normal and rotational stiffnesses. Note that the above formulation is physically meaningful only if the magnitutde of the relative displacements is infinitesimal.

The total contact forces and moments are in general made up of an elastic and a viscous part, so that:

$$\mathbf{F}^{ji} = \mathbf{F}^{ij}{}_{\text{el}} + \mathbf{F}^{ij}{}_{\text{vis}}, \tag{6}$$

$$\mathbf{M}^{ji} = \mathbf{M}^{ij}{}_{\text{el}} + \mathbf{M}^{ij}{}_{\text{vis}}. \tag{7}$$

In analogy to (4) and (5) we assume

$$\mathbf{F}^{ij}{}_{\text{vis}} = \eta_{s}\,(\mathbf{g}^{ji} - (\mathbf{g}^{ji}\cdot\mathbf{n}^{ji})\mathbf{n}^{ji}) + \eta_{s}\,(\mathbf{g}^{ji}\cdot\mathbf{n}^{ji})\mathbf{n}^{ji}, \tag{8}$$

$$\mathbf{M}^{ji}{}_{\text{vis}} = d^{ji2}\,\eta_{r}\,(\mathbf{s}^{j} - \mathbf{s}^{i}). \tag{9}$$

where η_s, η_n and η_r are constant tangent, normal and rotational viscosities.

The contact viscosities may have a real physical significance, eg for visco-elastic contacts or in fast granular flows. In the latter case, the viscosities are defined by the normal and tangent coefficients of restitution (Mühlhaus and Hornby, 1997). In connection with the solution of quasi-static problems by dynamic relaxation, the siginificance of the viscosities is purely numerical and the values of the viscosities are chosen exclusively in view of numerical efficiency.

In the 2D analyses intended here, $\mathbf{F}^{ji}$, $\mathbf{g}^{ji}$, $\mathbf{s}^{j}$ and $\mathbf{M}^{ji}$ have components (F_s^{ji}, F_n^{ji},0), (g_s^{ji}, g_n^{ji}, 0), (0,0, s^j), (0, 0, M^{ji}), respectively.

The contact yield criterion in the present model is illustrated in Figure 2, where C and f_T designate the cohesive force and tensile

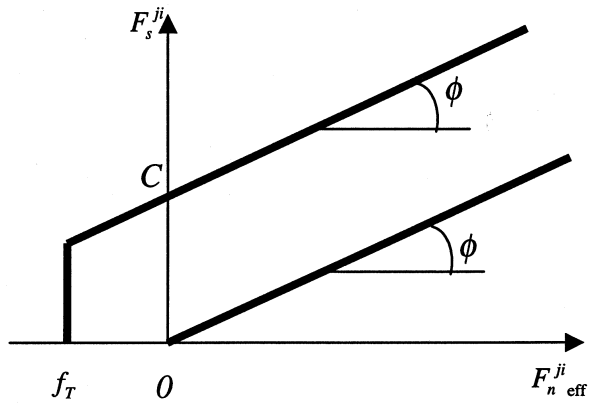

FIG 2 - Contact yield criterion.

strength of the contact, ϕ is Coulomb's angle of friction and $F_n^{ji}{}_{\text{eff}}$ is an effective normal force defined as:

$$F_{n\ eff}^{ji} = F_{n}^{ji} + \frac{2\alpha^{ji}}{d^{ji}}\left|M^{ji}\right|, \tag{10}$$

where $\alpha^{ji} \le 1$ is a dimensionless material parameter. Through the inclusion of the moment term in Equation 10 we consider the influence of possible load eccentricities with respect to the mathematical centre of the contact (a similar criterion was used by van Mier *et al*, 1996, within the context of a lattice model for concrete fracture). Upon initial yield *C* and f_T are put equal to zero and

$$F_s^{ji} = \tan\phi F_n^{ji}{}_{\text{eff}}. \tag{11}$$

Separation of the particles *i* and *j* occurs if the effective normal force $F_n^{ji}{}_{\text{eff.}} = 0$.

The configurations of the particles systems are determined as usual by integration of the equations of motion

$$\sum_{\text{contacts}} \mathbf{F}^{ji} + \gamma^{i} - \mathbf{m}^{i}\dot{\mathbf{v}}^{i} = 0 \tag{12}$$

and

$$\sum_{contacts} \left(\frac{1}{2}D^{i}\mathbf{n}^{ji}\times\mathbf{F}^{ji} + \mathbf{M}^{ji}\right) + \mu^{i} - \frac{1}{8}\mathbf{m}^{i}D^{i\,2}\dot{\mathbf{s}}^{i} = 0, \tag{13}$$

where $\mathbf{m}^{i}$ and D^{i} are the mass and diameter of the *i*-th particle; γ^{j} and μ^{i} are external particle forces and particle moments respectively.

Vertex centered finite difference scheme for fluid flow

Spatial discretisation and finite difference scheme

The formulation embodies full coupling between solid and fluid momentum transfer. A flow calculation is based on local porosities and permeabilities on a triangular mesh. As is depicted in Figure 3, the triangular mesh is generated by Delaunay triangulation connecting the mass centres of each particle and its nearest neighbours. For each triangular domain, the flowrate is calculated, as follows.

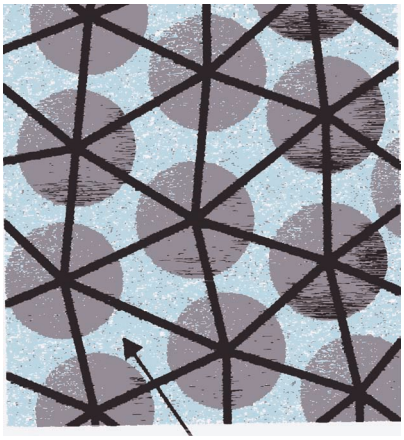

FIG 3 - Discretised space: Triangular mesh and particles.

The two-dimensional form of Gauss' divergence theorem applied to a function $\mathbf{F}(x_i)$ reads:

$$\int_s \mathbf{F}\mathbf{n}_i ds = \int_A \frac{\partial \mathbf{F}}{\partial_{xi}} dA \tag{14}$$

where S is the length of a closed loop, $\mathbf{n}_i$ is the outward unit normal of S, A is the area of a region surrounded by S, the average value of the gradient of the function

$$\frac{\partial \mathbf{F}}{\partial x_i}$$

over a small region A can be expressed as:

$$\left[\frac{\partial \mathbf{F}}{\partial_{xi}}\right]_{\text{ave}} = \frac{1}{A}\int_s \mathbf{F}\mathbf{n} ds \cdot \tag{15}$$

For a triangular region for A, the equation above may be approximated by:

$$\left[\frac{\partial \mathbf{F}}{\partial_{xi}}\right]_{\text{ave}} \approx \frac{1}{A}\sum_{ab=1}^{3} \mathbf{F}^{ab}\mathbf{n}_i^{ab}\Delta s^{ab}, \tag{16}$$

where Δs is the length of a side of the triangular region (Figure 4) and $(\bullet)^{ab}$ is the value of $(\bullet)$ at the centre of the side *ab*.

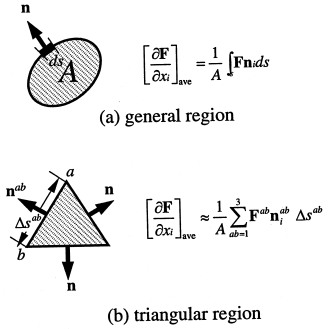

FIG 4 - Line integral over a small region.

For Darcy's law for a porous medium,

$$\mathbf{v}_i = K\frac{\partial P}{\partial_{xi}}, \tag{17}$$

where $\mathbf{v}_i$ is the specific discharge vector, $\boldsymbol{P}$ is the pressure and $\boldsymbol{K}$ is the permeability, we obtain for the average specific discharge vector over a small triangular region

$$\mathbf{V}_i \approx \frac{1}{A}\sum_{ab=1}^{3} K^{ab}P^{ab}\mathbf{n}_i^{ab}\Delta s^{ab}, \tag{18}$$

where

$$P^{ab} = \frac{P^a + P^b}{2} \tag{19}$$

In our model, the pressure $\boldsymbol{P}$ is treated as a nodal quantity and the permeability K may have a different values on each side of the triangular zone or element. If the contact force of a bond reaches the contact yield strength, then bond breakage takes place and the permeability of the respective side is increased correspondingly.

The flowrate through the side *ab* of the triangle *abc* in Figure 5 is the projection of the specific discharge $\mathbf{v}_i$ in the normal direction of the side *ab* multiplied by the length of ab, ∇s^{ab} as:

$$\mathrm{q}^{ab} = \mathbf{v}_i \cdot \mathbf{n}_\mathbf{i}^{\ ab}\,\Delta s^{\ ab} \tag{20}$$

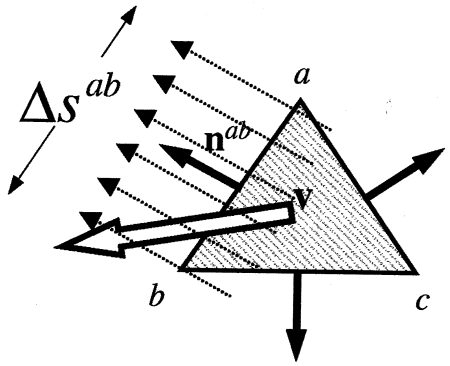

FIG 5 - Flowrate through the side ab.

where $\mathbf{n}_i^{ab}$ is the unit normal vector. Then, as in illustrated in Figure 6, the nodal flowrate is given as:

$$q^a = \frac{q^{ab}}{2} + \frac{q^{ca}}{2} \cdot \tag{21}$$

Consequently, the nodal flowrate is obtained from the nodal pressure for the triangular *abc*. Expressed in matrix notation we have:

$$\begin{bmatrix} q^a \\ q^b \\ q^c \end{bmatrix} = \begin{bmatrix} \ldots\ K^{ab}, K^{bc}, K^{ca}\ \ldots \\ \ldots\ \mathbf{n}_i^{\ ab}, \mathbf{n}_i^{bc}, \mathbf{n}_i^{\ ca}\ \ldots \\ \ldots \Delta s^{ab}, \Delta s^{bc}, \Delta s^{ca} \ldots \end{bmatrix} \begin{bmatrix} P^a \\ P^b \\ P^c \end{bmatrix} \tag{22}$$

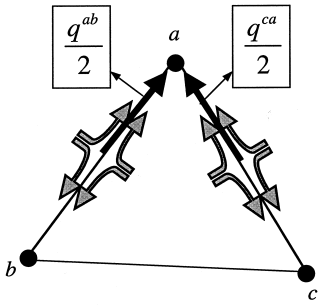

FIG 6 - Nodal flowrate.

As is depicted in Figure 7, one nodal point is generally shared by several triangles.

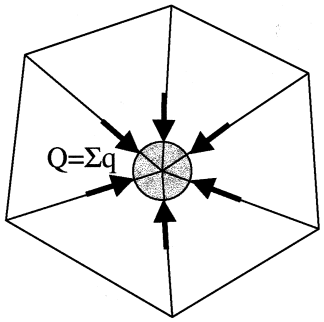

FIG 7 - Nodal flowrate Q.

The net nodal flowrate Q is the sum of q on the node of all the triangles.

$$Q = \sum q \tag{23}$$

Note that $Q = 0$ for incompressible flow. The fluid volume change ∇V_f is related to Q as:

$$\Delta V_f = Q\Delta t \cdot \tag{24}$$

In present notation the volumetric relation for a Biot coefficient of $\alpha = 1$ reads:

$$\Delta P = -B_w\left[\frac{Q}{V_f}\Delta t + \frac{\Delta V_p}{V_p}\right], \tag{25}$$

where V_f is the fluid volume contained in a cell and V_p is the pore volume (see Figure 8). We assume that $V_f\ (t = 0) = V_p$. Note that in our notation ∇V_f as ∇V_p are positive in extension. When the nodal pressure is updated by solving Equation 25, the pressures around the nodal points are momentarily kept constant. The matrix of the Crank-Nicholson scheme is then diagonal.

Mechanical coupling

The coupling between pore fluid flow and solid deformation occurs in three ways:

1. the deformation and bond fracture of the solid influences the permeability of the matrix material. Hydraulically, fractures are modelled as zones of high permeability;

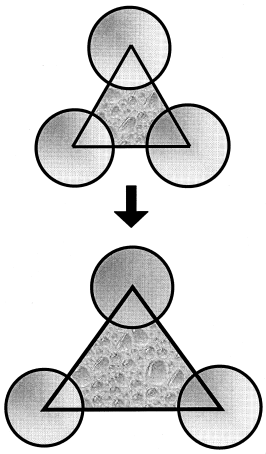

FIG 8 - Pore volume change.

2. the volume changes of the solid material are considered in the mass balance of the pore fluid; and
3. each particle includes in its momentum balance the resultant of the pore fluid surface tractions.

The first two items have already been discussed above. To consider the problem of applying the net fluid pressure force to a particle centre, we consider the polygon as depicted in Figure 9. We have

$$\mathbf{F}_p^i = \sum_{\text{surface}}\left(\frac{1}{2}L^{ji}(1-\varphi^{ji})(P^j + P^i)n^{ji}\right) \tag{26}$$

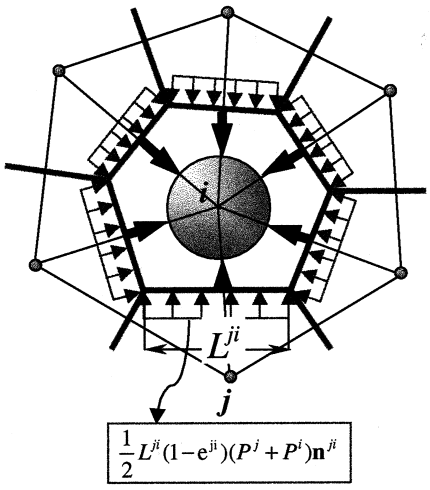

FIG 9 - Pore fluid surface tractions.

where P^i, P^j are nodal point pressures, L^{ji} is the length of the side of the Voronoi polygons intersecting the line connecting the mass centres of the particles i and j, φ^{ji} is the local porosity which depends on the stretch of the line connecting the mass centres of the particles i and j, and $\mathbf{n}^{ji}$ is the unit vector into the direction of the line. If the pressure around a particle i is uniform, then $\mathbf{F}^i_p = 0$.

The formulation above is based on compressible Darcy flow in porous media. Note that no restrictions other than $\alpha = 1$ (for a Biot coefficient) imposed regarding the compressibility of the pore fluid or gas. The theory therefore also holds for problems involving gas-solid interactions, in connection with the simulation of blasting operations. Because, as is seen in Equation 28, the fluid dealt in this method is compressible and vertex centred finite difference scheme itself is suitable for rapid flow.

Macro-particles

On the scale of grains and micro crack the structure of rock appears highly disordered and complex in general. A major advantage of the present model is that such complexities can be easily dealt with. A simple algorithm for the generation of complex shaped macro-particles is described in Mühlhaus *et al*, (1997), Sakaguchi and Mühlhaus, (1997).

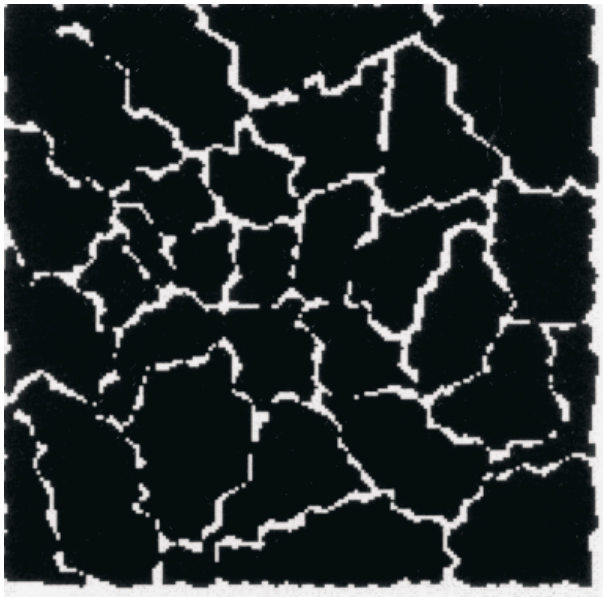

FIG 10 - Irregular shaped macro-particles.

Initially, seed particles are generated in a given domain by a uniform random process in which co-ordinate pairs are continuously determined until the total number of the seed particles reaches a preset value. Once all the seed particles are positioned, macro-particles are grown according to the random process from seed particles to fill the space. The resulting particles shapes are usually irregular (Figure 10) with a significant proportion of non-convex particle shapes. However, the proportion of convex particle shapes can be also controlled by using choosing growing direction (see Sakaguchi and Mühlhaus, 1997).

Assemblies of bonded macro-particles may represent for instance particular rock or ceramics fabrics, while assemblies of loose macro-particles are considered in fragmentation, comminution and flow problems involving angular granules.

EXAMPLES

Granular flow

Let us consider a rectangular domain, which has a trap door located at the centre of the bottom side, filled with randomly shaped, cohesionless particles (Figure 11) generated by the macro-particles generator which briefly described above section.

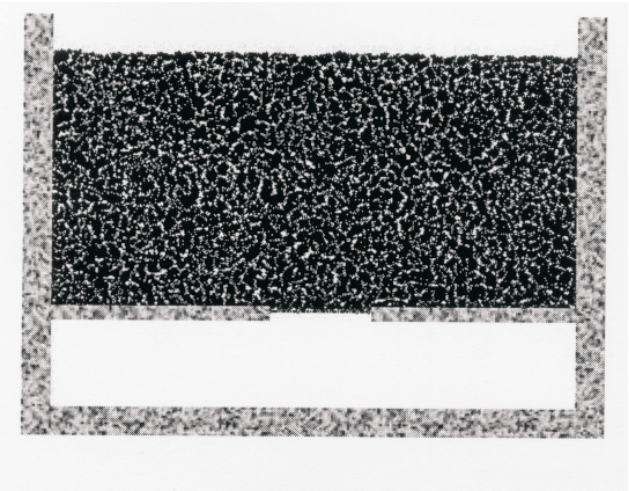

FIG 11 - Block caving - initial state.

This example could be a simplified model for mining of an orebody in block caving. Upon opening of a trap door centred at the lower side of the domain, granular flow set in and stops after a stable arch has formed above the trapdoor. Figure 12 shows the final equilibrium configuration.

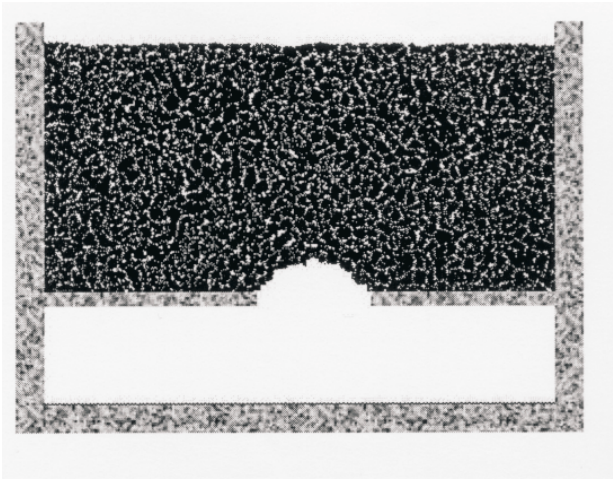

FIG 12 - Block caving - stable equilibrium configuration.

In the following example we demonstrate that the stability of the arch is determined by the ratio of the strength of the asperities of the macro-particles to the weight of the elemental particles. The initial particle configuration and the strength and elasticity properties are the same as in the above example. However the weight of the elemental particles is ten times higher. In this case the intensity of the asperity and particle fracture process is high enough to accommodate sustained granular flow. A snap shot of the discharge process is shown in Figure 13.

Blasting problems

In the following examples we demonstrate the applicability of the method introduced above to the simulation of blasting processes in a jointed rock mass. It is generally accepted that, although there have been substantial efforts over the past several decades, the mechanics and process of rock breakage by explosives are still poorly understood. This is mainly due to the

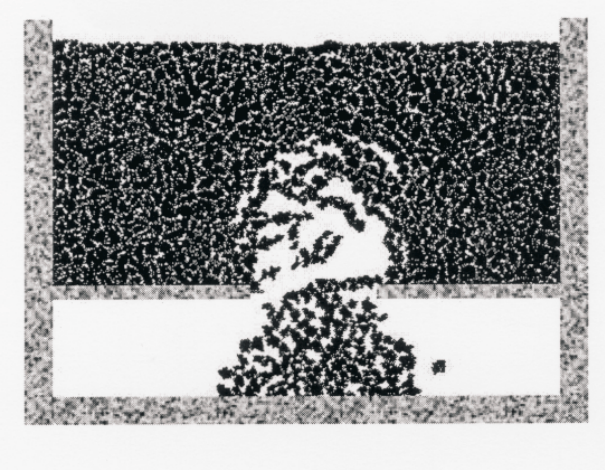

FIG 13 - Block caving - flow pattern for fracturing particles.

rapidity and complexity of the process. Mechanisms of rock fragmentation by blasting in terms of the relative significance of dynamic stress wave propagation and the so-called quasi-static gas pressurisation are still under debate. Rock structures such as joints, for example, further complicate the analysis.

Gas pressurisation effects

In our model analysis, we assume that the explosive loading is caused by two distinct mechanisms. First, the immediate rise time to the peak detonation pressure results in the propagation of intense compressive and shear waves through the model. Second, the tail of the pressure-time relationship corresponds to gas pressurisation effects. The assumed borehole pressure profile reflects the typical quasi-static nature of the borehole loading by explosives (Figure 14). The pressure reaches the peak value immediately after the detonation. After the peak the pressure decays linearly.

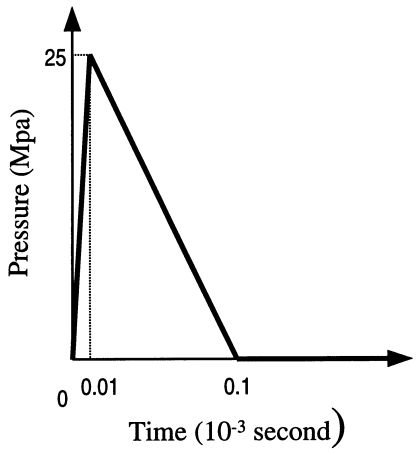

FIG 14 - Blasthole pressure - time relation.

Bench blasting in jointed rock

We consider two rows of blastholes in jointed rock (Figure 15). Problems of this kind are typical for the design of bench blasts in open pit mining. Five major joint surfaces are introduced with a spacing of 7.5 m and inclination of 30 degrees relative to the horizontal free surface. The time interval between detonations is again 0.1 ms.

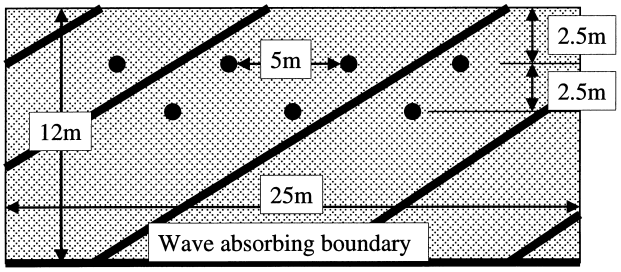

FIG 15 - Bench blasting in jointed rock.

Figure 16 illustrate the dynamic fracture history. It appears that at the early stage the fracture behaviour is mainly controlled by propagating stress waves. In the vicinity of the blastholes, a highly damaged zone, also known as the crushing zone, develops because of the intense lad imposed by the stress waves. Most cracks are arrested after a short period of time, mainly due to the attenuation of the stress waves and unfavourable dynamic states. However a number of major, localised fracture zones are clearly visible. The existence of the major fracture or damage zones is usually attributed to the action of the longer lasting gas pressurisation within the blast holes.

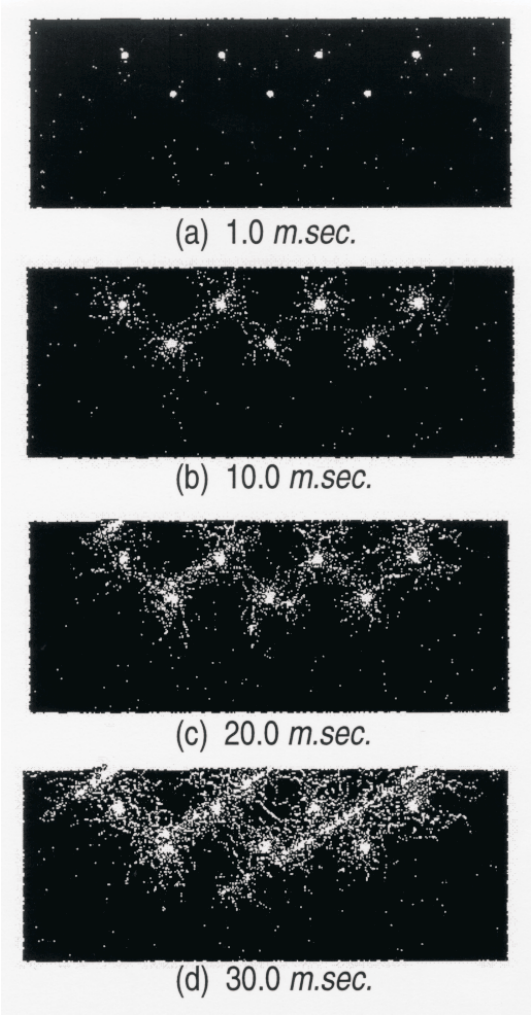

FIG 16 - Snapshots: Bench blasting in jointed rock.

The dynamic stress state changes when the propagating stress waves start interacting with the joints. Figure 16 shows clearly the intense fracturing in the vicinity of joints and the subsequent movement of fragments. Only limited transmission of cracks through joints is observed. This seems to indicate that the joints act similarly to open cracks or free surfaces. Since a compressive wave turns tensile after reflection from a free surface, fracture tends to occur in the form of spalling or tension cracks in the vicinity of the joints (Figure 16). Although the overall impact of joints on the fragmentation is yet to be quantified, it appears that joints have a significant effect on the fracture dynamics of bench blast operators. The latter is also confirmed by the results for a vertical cross-section shown in Figure 17.

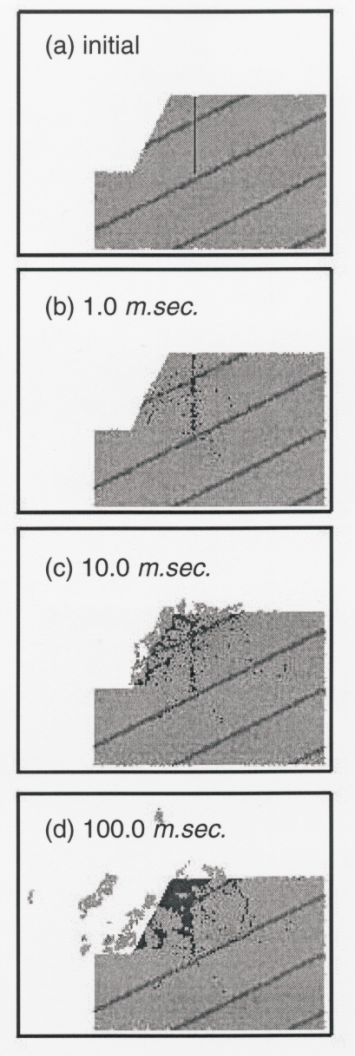

FIG 17 - Bench blasting: Vertical cross-section.

CONCLUSION

We have derived a new, incremental, particle based procedure coupling with fluid flow, intended for problems of deformation and fracture in rock blasting. The potential of the method was illustrated by means of example solutions related to granular flow and blasting in jointed rock. The blast modelling results are of qualitative nature but nevertheless reflect very well the overall features of the fractures and damage patterns as they are known from physical model tests.

ACKNOWLEDGEMENT

The support by the Centre of Offshore and Foundation Systems (COFS, UWA) is gratefully acknowledged through the collaboration to develop the discrete element modelling.

REFERENCES

Belytshko, T, Lu, Y Y and Gu L, 1994. Element free Galerkin methods, *Int Journal Numer Methods Eng*, 37:229-256.

Carter, B J, Ingraffea, A R and Bittencourt, T N, 1995. Topology-controlled modeling of linear and nonlinear 3D crack propagation in geomaterials, *Fracture of Brittle, Disordered Materials: Concrete, Rock and Ceramics*, (Eds: G Baker and B L Karihaloo) pp 301-318.

Cundall, P A and Strack, O D L, 1979. A discrete numerical model for granular assemblies, *Géotechnique*, 29:47-65.

Jirásek, M and Bazant, Z, 1993. Discrete element modelling of fracture and size effect in quasibrittle materials: Anyalysis of sea ice, in *Proceedings 2nd Int Conf DEM*, (Eds: J R Williams and G W Mustoe) pp 357-368.

Libersky, L D, Petschek, A G, Carney, A G, Hipp, T C and Allahdadi, F A, 1993. High strain Lagrangian hydrodynamics – A three-dimensional SPH code for dynamic material response, *Journal of Comput Phys*, 109:67-75.

Mühlhaus, H-B and Oka F, 1996. Dispersion and wave propagation in discrete and continuous models for granular materials, *International Journal of Solids and Structures*, 33(19):2841-2854.

Mühlhaus, H-B and Hornby, P, 1997. On the reality of antisymmetric stresses in fast granular flows, in *Proceedings IUTAM Conference on Granular and Porous Media*, (Eds: NA Fleck and Cocks), Kluwer.

Mühlhaus, H B, Sakaguchi, H and Wei, Y, 1997. Particle based modelling of dynamic fracture in jointed rock, *Computer Methods and Advances in Geomechanics*, (Ed: J-X Yuan) pp 207-216, (Balkema, Rotterdam/Brookfield).

Sakaguchi, H, Mühlhaus, H-B, 1997. Mesh free modelling of failure and localization in brittle rock, *Deformation and Progressive Failure in Geomechanics*, (Eds: Asoaka, Adachi, Oka) pp 15-21, (Pergamon).

Sakaguchi, H, 1995. Pattern formation in granular media, Doctoral Dissertation, Kyoto University.

Song, J and Kim, K, 1995. Numerical simulation of the blasting induced disturbed rock zone using the dynamic lattice network model, *Proceedings of 2nd International Conference on Mechanics of Jointed and Faulted Rock* (Ed: H-P Rossmanith) pp 755-761 (Balkema: Rotterdam).

Sulsky, D, Zhou, S-J and Schreyer, H L, 1995. Application of a particle-in-cell method to solid mechanics, *Comput Phys Commun*, 87:236-252.

van Mier, J G M, Schlangen, E and Vervurt, A, 1995. Lattice type fracture models for concrete, *Continuum Models for Material with Microstructure* (Ed: H-B Mühlhaus), pp 341-377, (Wiley).